IOP Conference Series: Materials Science and Engineering

PAPER • **OPEN ACCESS**

Effect of tempering on microstructure and mechanical properties of a Ta-added 9%Cr steel with high B and low N contents

To cite this article: E Tkachev and A Belyakov 2019 *IOP Conf. Ser.: Mater. Sci. Eng.* **525** 012049

IOP Conf. Series: Materials Science and Engineering **525** (2019) 012049 doi:10.1088/1757-899X/525/1/012049

Effect of tempering on microstructure and mechanical properties of a Ta-added 9%Cr steel with high B and low N contents

E Tkachev[1], A Belyakov[2]

[1,2]Belgorod State University, Belgorod 308015, Russia

E-mail: tkachev_e@bsu.edu.ru

Abstract. Ta was added to a modified 9%Cr steel with high B and low N content to achieve an optimal dispersion of second phase particles. The effect of tempering on the microstructure and mechanical properties of an Fe-0.1C-9Cr-1.8W-0.6Mo-3Co-Nb-V-0,0013B-0,007N-0,085Ta steel was investigated. Typical martensite lath structure was observed after normalization at 1323 K for 0.5 h. The $M_{23}(C,B)_6$ and complex (Nb,Ta)(C,N) particles formed during tempering at 1023-1053 K. An increase in the hardness after tempering at 1038 K was attributed to the precipitation of the fine (Nb,Ta)(C,N) particles. The impact toughness depended significantly on tempering temperature. The impact toughness increased from 25 to 181 J/cm^2 with increasing the tempering temperature from 1038 to 1053 K.

1. Introduction

9%Cr martensitic steels are an important class of structural materials for elevated temperature applications because of combination of good corrosion resistance and high creep strength. Several concepts have been proposed for the development of new creep-resistant steels with increased creep resistance [1-5]. Recently, considerable interest was paid to boron containing 9-10%Cr steels. A small amount of B was found useful to improve the stability of tempered martensite lath structure (TMLS) under creep conditions especially due to fine dispersion of $M_{23}(C,B)_6$ particles [6-8]. However, the nitrogen content in B-containing steels should be controlled to avoid the formation of BN particles [9,10]. In addition, Co is known as substitutional element, which is important to suppress the δ-ferrite formation during high temperature normalization. Since the newest B-containing steels contain 9-10%Cr and 2-2,5%(W+Mo), the optimum Co content required to avoid the δ-ferrite formation was found to be ~3% [1,11,12]. Following this alloying design, several 9-10%Cr steels with increased creep strength were developed [13-15].

It is well known that MX-type carbonitride particles play an important role in creep resistance due to their fine dispersion and increased stability. Ta is a strong carbide/nitride forming element and is widely used to replace the Nb in reduced activation ferritic-martensitic (RAFM) steels, which are used in fusion power plant components. It was reported that in 9%Cr steel Ta formed fine TaC particles, which are smaller than those in steels without Ta [16]. Thus, in order to further improve the high temperature strength the combined addition of B and Ta was suggested.

The precipitation behavior and mechanical properties of high-chromium martensitic steels are closely connected with tempering temperature. Thus, the present work describes the effect of tempering on microstructure and mechanical properties of a modified Ta-added 9% Cr steel with high B and low N contents.

2. Materials and method

A modified 9%Cr-3%Co-2%W steel was produced by vacuum induction melting. The chemical composition of the steel is given in table 1. The steel samples were normalized at 1323 K for 0.5 h and tempered at 1023; 1038 and 1053 K for 3 h.

Table 1. Chemical composition of the studied steel (wt.%).

C	Ni	Mn	Cr	W	Mo	Nb	V	Co	Ta	N	B	Fe
0.11	0.02	0.30	9.05	1.99	0.61	0.06	0.19	3.06	0.085	0.007	0.013	Bal.

The microstructures of the present steel were analysed by optical microscopy and transmission electron microscopy (TEM) using Jeol JEM-2100 microscope operating at 200kV equipped with an INCA energy-dispersive X-ray (EDX) spectrometer. The dislocation densities were estimated by counting the individual dislocations in the lath interiors per unit area on arbitrarily selected TEM images. Extraction carbon replicas were prepared to determine the size distribution of different types of precipitates. The fracture surface of the impact tested specimens has been studied by using the FEI Nova NanoSEM 250 scanning electron microscope (SEM).

The hardness of studied steel after normalization and tempering was measured using Brinell tests with a load of 750 N and a ball diameter of 5 mm. Impact tests were performed at room temperature on an Instron IMP460 impact testing machine using standard 10×10×55 mm^3 specimens with a 2 mm V-notch.

3. Results and discussion

3.1. Microstructure after normalization and tempering

3.1.1. Microstructure of normalized steel The optical metallography showed that after normalization at 1323 K for 0.5 h the studied steel had a fully martensite microstructure without delta ferrite (figure 1). The mean size of prior austenite grains in this condition was 54±3 μm.

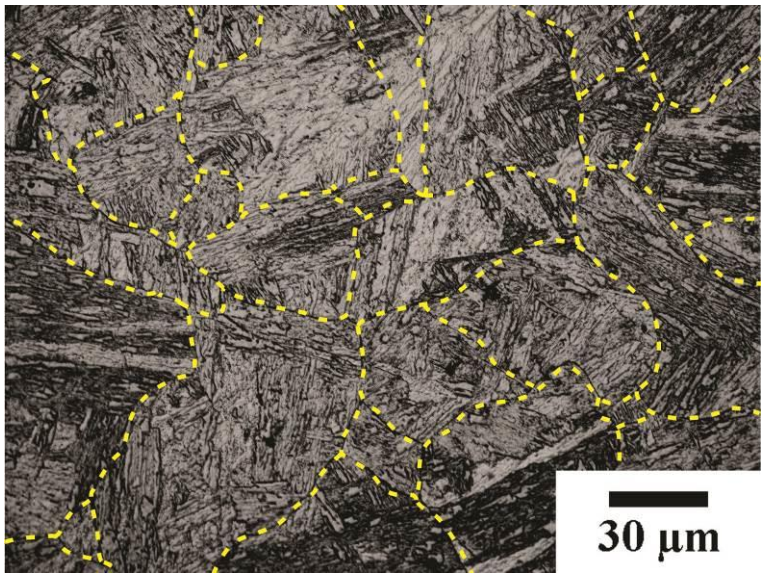

Figure 1. Optical image of the etched surface of the steel after normalization at 1323K for 0.5 h. The prior austenite grain boundaries are indicated by yellow dash lines.

The TEM observation revealed the lath martensite hierarchical substructure with an average lath thickness of 190±20 nm (figure 2). The high dislocation density of 4.5×10^{14} m^{-2} arisen from γ→α transformation was maintained in the studied steel after normalization.

Similar to the previous studies on the effect of normalization and tempering on the structure of 9%Cr steels [17.18], the Fe_3C particles formed during cooling after austenization were observed in the studied steel (figure 2).

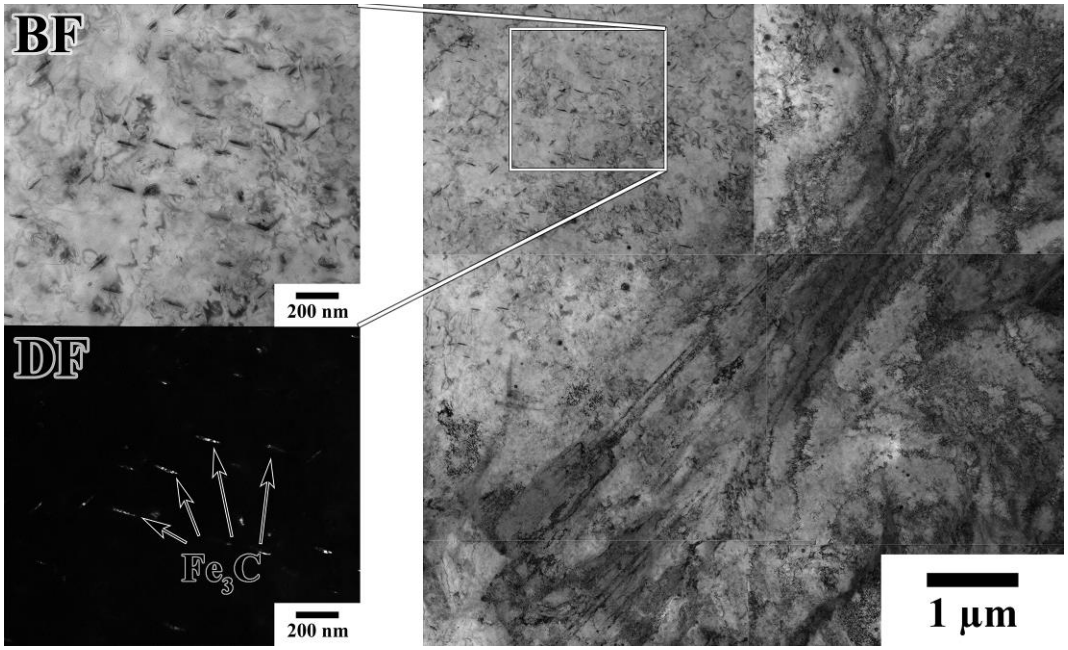

Figure 2. TEM microstructure of the steel after normalization at 1323 K for 0.5 h. The magnified bright field image (BF) and dark field image (DF) show the plate-like particles of cementite.

These particles has plate-like shape with mean size of 75×13 nm and arranged parallel to each other which suggests the presence of preferential crystallographic orientation relationship between these particles and α-martensite. In addition, the (Nb,Ta)(C,N) particles with round shape and mean size of 38 nm were observed.

3.1.2. Microstructure after tempering The tempering led to significant increase of the lath width (table 2). The lath widening was accompanied by the rearrangement of dislocation structure and the particle precipitation. Thus, the dislocation density gradually decreased to 0.9×10^{14} m^{-2} with increasing tempering temperature to 1053 K. Typical TEM micrographs of the studies steel after tempering at different temperatures are shown in figure 3.

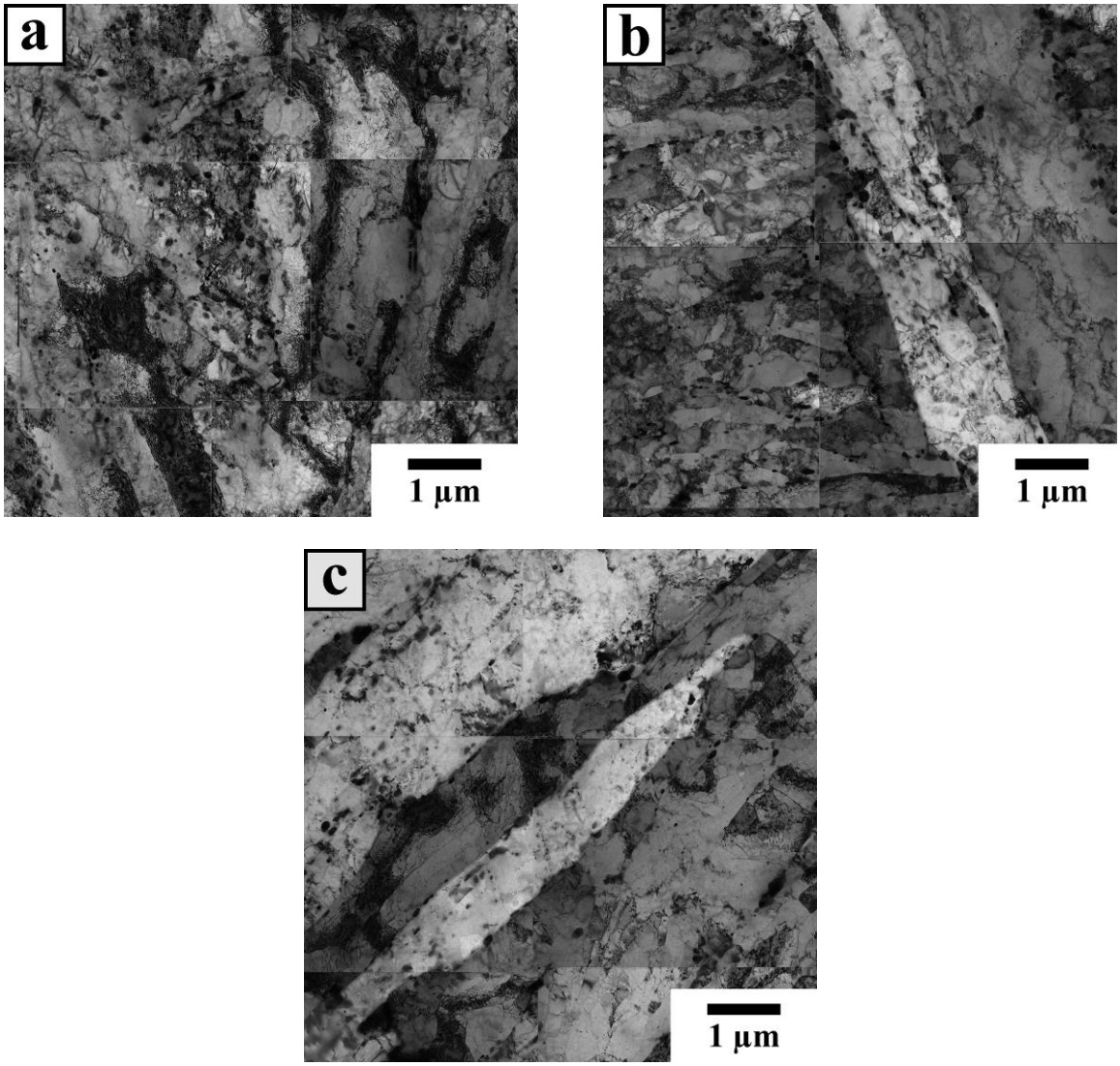

Figure 3. TEM micrographs of the steel after tempering at 1023 K (a); 1038 K (b) and 1053 K (c) showing the TMLS with decoration of $M_{23}(C,B)_6$ carbides on lath boundaries.

The main parameters of the tempered martensite lath structures (TMLS) and the mean diameters of each precipitate are represented in table 2. The tempering led to dissolution of Fe_3C particles. The major observed phase in the tempered conditions was $M_{23}(C,B)_6$ carbide which is more stable than cementite. The most of $M_{23}(C,B)_6$ particles are located along the lath and PAG boundaries and there is no significant difference in the size of these particles among the three steel specimens tempered at 1023; 1038 and 1053 K.

Table 2. Parameters of the microstructure after normalization and tempering at different temperatures.

Tempering Temperature	Normalized	1023 K	1038 K	1053 K
Lath width, nm	190±20	270±15	305±25	355±35
Dislocation density, $\times 10^{14}$ m^{-2}	4.5	3.5	2.4	0.9

Average size of Fe_3C, nm	75×13	-	-	-
Average size of $M_{23}(C,B)_6$, nm	-	71	75	80
Average size of (Nb,Ta)(C,N), nm	38	26	19	21

In order to clarify the precipitation behavior of (Nb,Ta)(C,N) particles, the size distribution histograms were analyzed (figure 4). It can be seen that undissolved primary particles of (Nb,Ta)(C,N) maintained in steel in normalized condition while additional fine particles of (Nb,Ta)(C,N) precipitate during subsequent tempering. The early-stage precipitation of the secondary (Nb,Ta)(C,N) particles was observed after tempering at 1023 K. The minimum size of these particles was found to be less than 10 nm. Increasing tempering temperature to 1038 K enhanced the precipitation of (Nb,Ta)(C,N) particles and, thereby, decreased the mean size of total population of these particles.

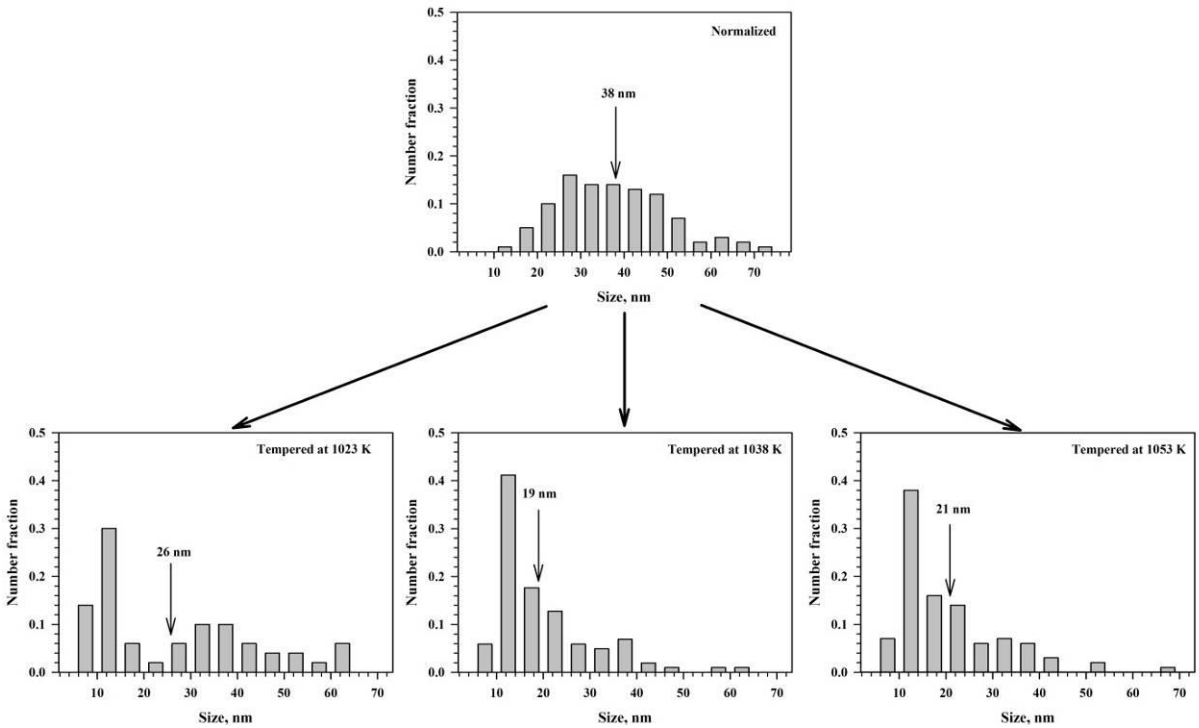

Figure 4. The size distribution of (Nb,Ta)(C,N) particles after tempering at 1023; 1038 and 1053 K. The mean size values are indicated by arrows.

EDX analysis showed that Nb/Ta ratio in (Nb,Ta)(C,N) particles was nearly equal to 50/50 at%. However, it should be noted that in contrast to the coarse primary (Nb,Ta)(C,N) particles, the fine secondary particles of this phase are characterized by increased Fe and Cr content as illustrated in figure 5.

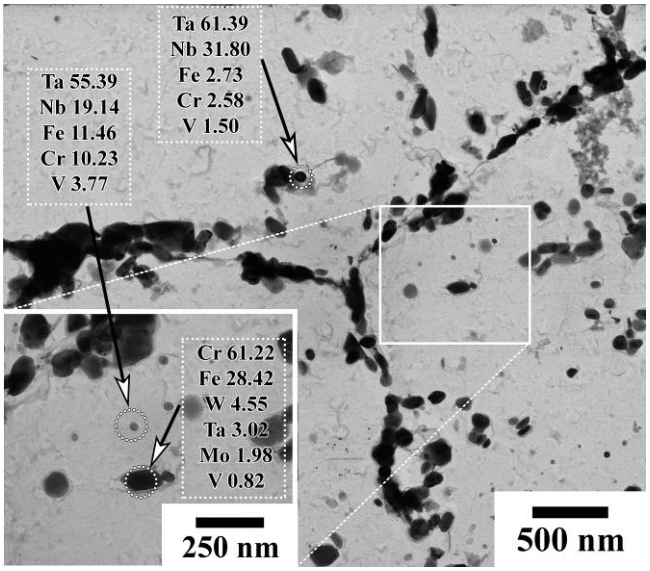

Figure 5. TEM image of dispersed particles that evolved after tempering at 1053 K for 3h. The compositions of particles are shown in wt%.

3.2. *Hardness, impact tests and fractography* The influence of tempering temperature on mechanical behaviour of the studied steel, including hardness and impact toughness, is represented in figure 6.

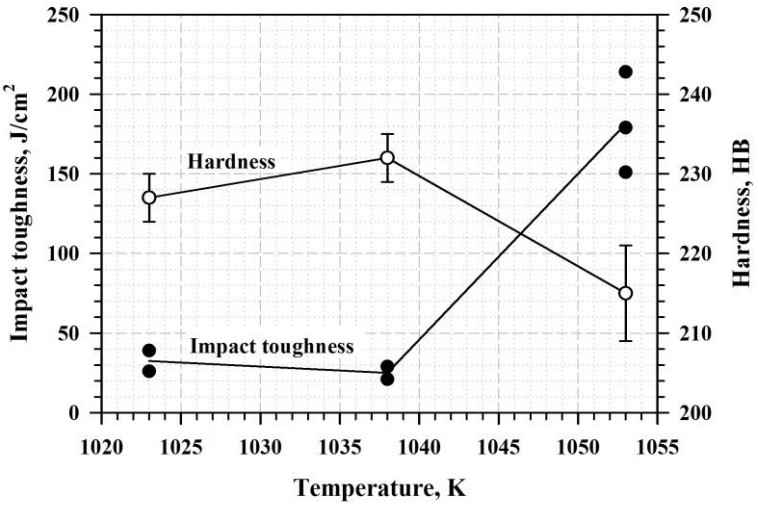

Figure 6. Impact toughness and Brinell hardness of the studied steel tempered at different temperatures.

The hardness of the studied steel after tempering at 1038 K was slightly increased as compared to that after tempering at 1023 K that might be caused by the secondary precipitations. A marked decrease of hardness occured after tempering at 1053 K. This can be attributed to the lath widening and a decrease in the dislocation density. In contrast to hardness, the toughness of the studied steel reached its minimum value of about 25 J/cm^2 after tempering at 1038 K. After tempering at 1053 K the studied steel displaied the high value of impact energy of 181 J/cm^2. Such a significant change in

the toughness led to quite different morphology of the fractured surfaces (figure 7), that is much similar to other studies [19,20].

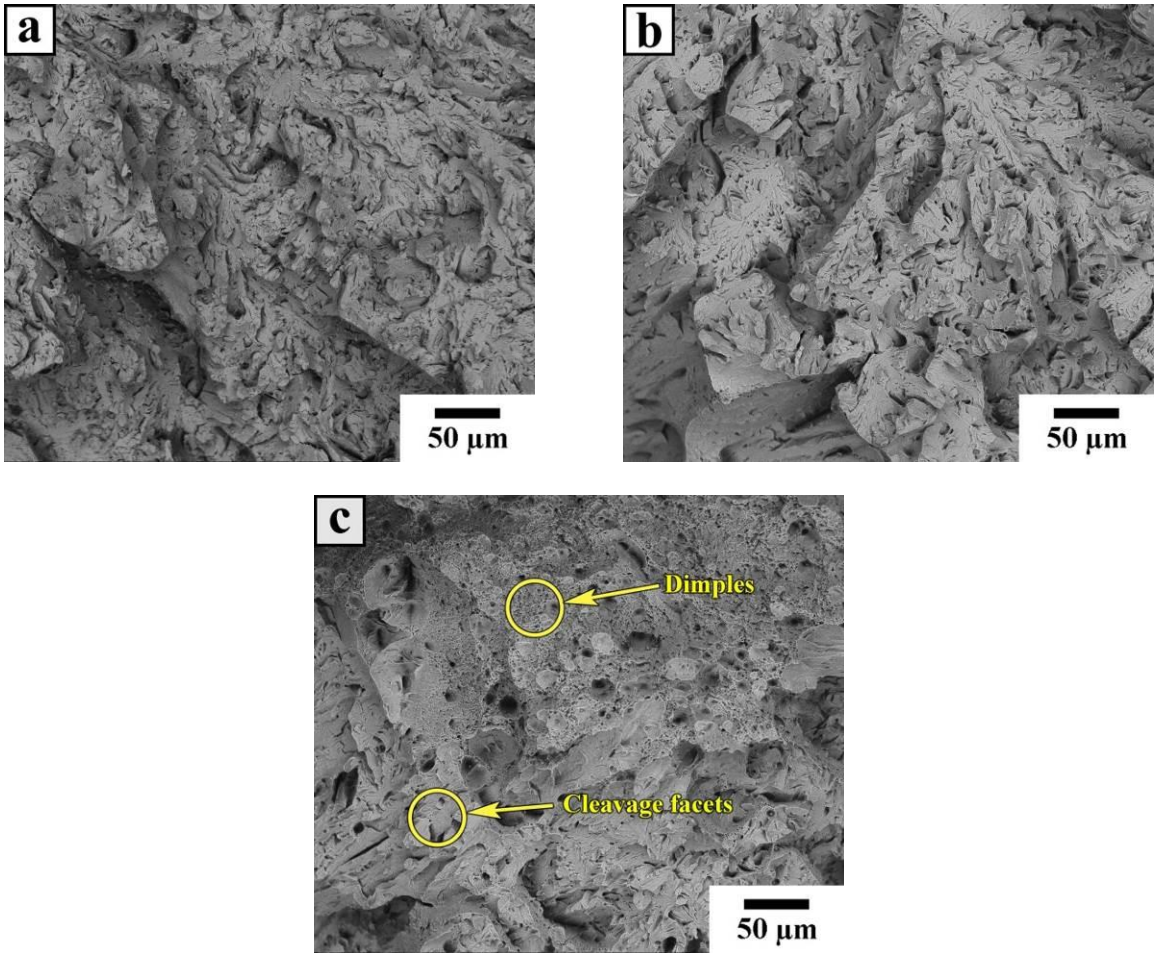

Figure 7. SEM fractographs in crack propagation zone of the studied steel after tempering at 1023 K (a); 1038 K (b) and 1053 K (c).

The SEM analysis of the fractured surfaces of broken Charpy impact specimens revealed the brittle cleavage fracture of the steel samples tempered at 1023 and 1038 K. However, the size of the cleavage facets of the sample tempered at 1023 K is smaller and more irregular, thus the propagation direction of the cleavage crack was deflected more frequently resulting in higher impact toughness. The fracture surface in crack propagation zone of the sample tempered at 1053 K is characterized by presence of ductile dimples tearing along with flat cleavage facets. This indicates the mixed mode of the fracture mechanism.

4. Summary and conclusions

The microstructure and mechanical behavior of a Ta-added 9Cr martensitic steel with high B and low N contents were investigated after normalization and tempering. The following key conclusions can be drawn:

1. The normalization resulted in full martensite structure with thin laths and high dislocation density. The observed secondary phase particles were identified as primary MX-type particles of (Nb,Ta)(C,N) with round shape and Fe_3C platelets.

2. Tempering at 1023-1053 K led to the precipitation of $M_{23}(C,B)_6$ and the secondary (Nb,Ta)(C,N) particles. The most pronounced precipitation of the secondary (Nb,Ta)(C,N) particles was observed at a temperature of 1038 K as revealed by an increase of hardness due to precipitation hardening.
3. Tempering at 1053 K is the most suitable regime for the studied steel because of optimum combination of hardness and toughness.

Acknowledgement
The reported study was funded by RFBR according to the research project № 18-38-00052.

References
[1] F. Abe, T.U. Kern, R. Viswanathan, Creep-Resistant Steels, 2008. doi:10.1533/9781845694012.
[2] F. Abe, M. Taneike, K. Sawada, Alloy design of creep resistant 9Cr steel using a dispersion of nano-sized carbonitrides, Int. J. Press. Vessel. Pip. **84** (2007) 3–12. doi:10.1016/j.ijpvp.2006.09.003.
[3] F. Abe, Precipitate design for creep strengthening of 9% Cr tempered martensitic steel for ultra-supercritical power plants, Sci. Technol. Adv. Mater. **9** (2008) 013002. doi:10.1088/1468-6996/9/1/013002.
[4] R.O. Kaybyshev, V.N. Skorobogatykh, I. a. Shchenkova, New martensitic steels for fossil power plant: Creep resistance, Phys. Met. Metallogr. **109** (2010) 186–200. doi:10.1134/S0031918X10020110.
[5] Z. Hong, X. Zhang, Q. Yan, Y. Chen, A new method for preparing 9Cr-ODS steel using elemental yttrium and Fe2O3oxygen carrier, J. Alloys Compd. **770** (2019) 831–839. doi:10.1016/j.jallcom.2018.08.196.
[6] R. Sahara, T. Matsunaga, H. Hongo, M. Tabuchi, Theoretical Investigation of Stabilizing Mechanism by Boron in Body-Centered Cubic Iron Through (Fe,Cr)23(C,B)6Precipitates, Metall. Mater. Trans. A Phys. Metall. Mater. Sci. **47** (2016) 2487–2497. doi:10.1007/s11661-016-3397-7.
[7] F. Abe, Effect of boron on creep deformation behavior and microstructure evolution in 9 % Cr steel at 650°C, Int. J. Mater. Res. **99** (2008) 387–394. doi:10.3139/146.101650.
[8] N. Dudova, R. Mishnev, R. Kaibyshev, Effect of Tempering on Microstructure and Mechanical Properties of Boron Containing 10%Cr Steel, ISIJ Int. **51** (2011) 1912–1918. doi:10.2355/isijinternational.51.1912.
[9] E. El-Kashif, K. Asakura, K. Shibata, Effects of Nitrogen in 9Cr-3W-3Co Ferritic Heat Resistant Steels Containing Boron., ISIJ Int. **42** (2002) 1468–1476. doi:10.2355/isijinternational.42.1468.
[10] L. Li, R. MacLachlan, M.A.E. Jepson, R. Thomson, Microstructural evolution of boron nitride particles in advanced 9Cr power plant steels, Metall. Mater. Trans. A Phys. Metall. Mater. Sci. **44** (2013) 3411–3418. doi:10.1007/s11661-013-1642-x.
[11] Å. Gustafson, J. Ågren, Possible Effect of Co on Coarsening of M23C6 Carbide and Orowan Stress in a 9% Cr Steel., ISIJ Int. **41** (2001) 356–360. doi:10.2355/isijinternational.41.356.
[12] L. Helis, Y. Toda, T. Hara, H. Miyazaki, F. Abe, Effect of cobalt on the microstructure of tempered martensitic 9Cr steel for ultra-supercritical power plants, Mater. Sci. Eng. A. **510-511** (2009) 88–94. doi:10.1016/j.msea.2008.04.131.
[13] E. Tkachev, A. Belyakov, R. Kaibyshev, Creep behavior and microstructural evolution of a 9%Cr steel with high B and low N contents, Mater. Sci. Eng. A. **725** (2018). doi:10.1016/j.msea.2018.04.032.
[14] A. Fedoseeva, I. Nikitin, N. Dudova, R. Kaibyshev, On effect of rhenium on mechanical properties of a high-Cr creep- resistant steel, Mater. Lett. **236** (2019) 81–84. doi:10.1016/j.matlet.2018.10.081.
[15] R. Mishnev, N. Dudova, R. Kaibyshev, On the origin of the superior long-term creep resistance of a 10% Cr steel, Mater. Sci. Eng. A. **713** (2018) 161–173. doi:10.1016/j.msea.2017.12.066.

[16] F. Abe, Bainitic and martensitic creep-resistant steels, Curr. Opin. Solid State Mater. Sci. **8** (2004) 305–311. doi:10.1016/j.cossms.2004.12.001.
[17] W.B. Jones, C.R. Hills, D.H. Polonis, Microstructural evolution of modified 9Cr-1Mo steel, Metall. Trans. A. **22** (1991) 1049–1058. doi:10.1007/BF02661098.
[18] I. Fedorova, A. Kostka, E. Tkachev, A. Belyakov, R. Kaibyshev, Tempering behavior of a low nitrogen boron-added 9%Cr steel, Mater. Sci. Eng. A. **662** (2016) 443–455. doi:10.1016/j.msea.2016.03.092.
[19] V. Dudko, A. Fedoseeva, R. Kaibyshev, Ductile-brittle transition in a 9% Cr heat-resistant steel, Mater. Sci. Eng. A. **682** (2017) 73–84. doi:10.1016/j.msea.2016.11.035.
[20] V. Dudko, J. Borisova, R. Kaibyshev, Ductile-Brittle Transition in Martensitic 12 % Cr Steel, Acta Phys. Pol. A. **134** (2018) 10–13. doi:10.12693/APhysPolA.134.649.